


ARTICLE

<https://doi.org/10.1038/s42004-019-0230-4>

OPEN

Harmonic light scattering study reveals structured clusters upon the supramolecular aggregation of regioregular poly(3-alkylthiophene)

Michèle Moris^{1*}, Marie-Paule Van Den Eede², Guy Koeckelberghs², Olivier Deschaume ³, Carmen Bartic³, Stijn Van Cleuvenbergen^{4*}, Koen Clays¹ & Thierry Verbiest¹

Solubilized poly(3-alkylthiophene)s are known to self-assemble into well-ordered supramolecular aggregates upon lowering the solvent quality. This supramolecular organization largely determines the optical and electronic properties of these polymers. However, despite numerous studies the exact mechanism and kinetics of the aggregation process and the role of external stimuli are still poorly understood. Classical characterization techniques such as electronic spectroscopy, dynamic light scattering, and diffraction-based techniques have not been able to provide a full understanding. Here we use second-harmonic scattering (SHS) and third-harmonic scattering (THS) techniques to investigate this supramolecular aggregation mechanism. Our results indicate that the actual supramolecular aggregation is preceded by the formation of structured polymer-solvent clusters consistent with a nonclassical crystallization pathway.

¹Department of Chemistry, Molecular Imaging and Photonics, KU Leuven, Celestijnenlaan 200D, 3001 Heverlee, Belgium. ²Department of Chemistry, Polymer Chemistry and Polymer Materials, KU Leuven, Celestijnenlaan 200F, 3001 Heverlee, Belgium. ³Department of Physics and Astronomy, Soft-Matter Physics and Biophysics Section, KU Leuven, Celestijnenlaan 200D, 3001 Heverlee, Belgium. ⁴Department of Chemistry, Physical Chemistry, KU Leuven - KULAK, Etienne Sabbelaan 53, 8500 Kortrijk, Belgium. *email: michele.moris@kuleuven.be; stijn.vancluvenbergen@kuleuven.be

Conjugated polymers have received a lot of interest due to their interesting optoelectronic and photophysical properties. It is well-established that their properties strongly depend on their supramolecular organization, both in solution as well as in thin film or bulk. Hence, supramolecular organization of conjugated polymers has been a topic of great interest and debate. For example, numerous studies have been devoted to their supramolecular aggregation in good or poor solvents^{1–4} and in thin films^{5,6}, and to the influence of parameters such as temperature^{7–9}, pH or molecular structure^{10–13}. A particularly popular polymer system is polythiophene and its derivatives¹⁴. Although for applications the organization of the polymer in the solid phase is critically important, this organization is often dictated or influenced by the solvent from which the solid phase (often a spin coated film) is prepared^{15–17}. Indeed, the quality of the solvent in terms of solubility parameters, ratio of solvent to non-solvent, vapor pressure/boiling point, all play an important role in obtaining the final structure in the solid phase. Typical experiments consist of the polythiophene being dissolved in a good solvent, followed by lowering the quality of the solvent by decreasing the temperature, or by adding additives or non-solvent. This decrease in solubility triggers a supramolecular aggregation process, the onset of which is typically visualized by a color change resulting from a red-shift of the UV/Vis absorption spectrum or a change in fluorescence emission spectrum. For chiral polymers, circular dichroism (CD) is often used to obtain additional information on the aggregation process². These spectral changes are generally attributed to a phase separation resulting in two distinct phases in solution, i.e. coiled polymer in solution and planar polymer in the form of (semi-)microcrystalline aggregates^{9,18,19}. The consensus is that chain planarization and interchain π - π stacking in these well-ordered aggregates generate an increase in conjugation length explaining the concomitant changes in optical properties. For chiral polymers, Bouman et al.²⁰ found that chiral substituents can induce optical activity of the π - π^* transition only when the polymer is in a well-ordered aggregated state, and the final aggregates are believed to consist of helically stacked conjugated polymers.

Owing to the impact of structural organization on the physical properties of materials, systematic progress in structural control requires a fundamental insight in the mechanisms underlying phase separation and crystallization. While numerous studies²¹ have been devoted to the stimuli triggering phase separation in polythiophene solutions, and their effect on the optical properties and organization in films, the first stages of this process are still poorly understood. For many years it was thought that characterization of the final macroscopic structure provides a direct link to the nucleation process. Indeed, classical nucleation theory assumes that the initially formed nanoscopic nuclei adopt the same structure as the emerging macroscopic crystal phase, and that growth occurs by inclusion of monomeric particles^{22,23}. Although classical nucleation theory is still the most widely adopted theoretical model, its general applicability has come under serious scrutiny over the last decade^{24–27}. Experimental observations for biominerals, ionic species, small organic molecules, and proteins have made increasingly clear that supramolecular clusters, with sizes ranging from the subnanometer scale for inorganic molecules to several hundreds of nanometers for organic molecules and proteins often play a central role in nucleation processes^{24,28,29}. These species can act as nucleation precursors or growth species and do not fit within the framework of classical nucleation theory.

Alternative models have been suggested to explain the role of supramolecular clusters in nonclassical crystallization pathways. In the two-step model the formation of dense liquid clusters is considered as a primary step in a liquid-liquid demixing process,

after which transformation into a crystalline nucleus takes place within the clusters^{27,30}. Alternatively, the formation of supramolecular aggregates can be explained through the pre-nucleation cluster pathway^{24,25}. Pre-nucleation clusters are soluble, dynamic and thermodynamically stable entities which may have internal structure resembling that of the nascent crystal, and act as precursors to the phase nucleating from solution. They are equilibrium species and there is as such no phase boundary with the surrounding solution as in the two-step model.

Despite the growing body of evidence for the role of supramolecular clusters in nonclassical crystallization pathways, many open questions relating to their dynamics, thermodynamics, role of the solvent, and internal structure remain unanswered. Experimentally, the appearance of clusters can be detected with standard techniques such as static and dynamic light scattering (SLS and DLS) since they often emerge in relatively high concentrations due to their thermodynamic (meta)stability. However, determination of their internal structure in solution, a key part of the puzzle, is challenging and currently relies either on highly specialized nanometer-scale imaging using in-situ liquid cell transmission electron microscopy (TEM) and cryo-TEM^{31,32}, or on ensemble-averaged X-ray or neutron-based techniques with structural sensitivity, such as SAXS/WAXS³³.

Here we report an approach based on second- and third-harmonic light scattering to study the internal structure of relevant species involved in the aggregation and phase separation of regioregular poly(3-alkylthiophene) (P3AT) derivative *in situ*. These nonlinear optical light scattering techniques are inherently sensitive to symmetry and have been used to probe the structure of molecules³⁴, clusters, aggregates³⁵, and crystals^{36–40}. Although these optical techniques do not offer the nanometer resolution of some X-ray or neutron-based scattering techniques, they have the advantage that they do not require long-range order (e.g. over a number of unit cells as for diffraction-based techniques) to elicit structural information. Indeed, even monomeric species generate a nonlinear light scattering response that is different than that of dimeric aggregates^{41,42}. For the latter, the response will moreover depend on the relative orientation of the constituent monomers, giving insight in the aggregate structure⁴¹. By combining nonlinear light scattering with dynamic light scattering (DLS) and electronic spectroscopy techniques, we are able to study aggregation processes in a regioregular P3AT (semi-)microcrystalline phase *in situ*, and provide experimental evidence for the role of structured clusters in the supramolecular organization of these systems.

Results

Electronic spectroscopy. We first characterized the regioregular poly(3-alkylthiophene) (P3AT) (Fig. 1) supramolecular aggregation process using a combination of UV/Vis and CD

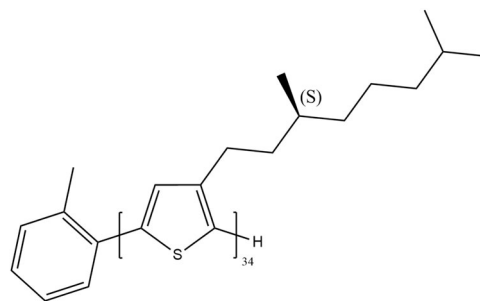


Fig. 1 Structure of regioregular poly(3-(3(S),7-dimethyl)thiophene). The used poly(3-alkylthiophene) consists of 34 monomeric units and has a dispersity of 1.1

spectroscopy. Initially when the polymer is in a good solvent, the polymer is generally assumed to be present in a non-aggregated state where it prefers an extended conformation owing to its rigid backbone^{2,4,7,43–47}. The featureless absorption band with a maximum at 448 nm is typically taken as a sign that aggregation is absent. In this state, the polymer is also highly fluorescent. The two-photon emission spectrum is similar to one-photon emission with a maximum at 580 nm. No CD can be observed in the visible part of the spectrum, again indicative of the absence of aggregation. Upon addition of small amounts (<33% v/v) of methanol (which is from now on referred to as the low methanol regime), which is a non-solvent for the polymer, no changes in UV/Vis or fluorescence are observed and a CD signal remains absent in the visible part of the spectrum (Fig. 2). In fact, the shape and magnitude of the UV/Vis absorption band are identical, independent of the amount of methanol added in this regime. The emission maximum of multiphoton fluorescence (MPF) (see further) which is collected simultaneously with the harmonic scattering is constant for small additions of methanol indicating that no aggregation is present.

Only upon addition of larger amounts of methanol (>33% v/v), UV/Vis, emission and CD all change (Fig. 2). The UV/Vis spectrum red shifts when the amount of methanol added is larger than approximately 33% and a vibrational fine structure appears in the spectrum, indicative of (semi-)crystalline aggregates (fully grown species)^{9,11,15,17}. This transition has been described in numerous studies in solution and thin film and is usually taken as a sign of the onset of aggregation and planarization of the

polymer backbone resulting in increased conjugation. Simultaneously, the fluorescence is quenched and a strong bisignate CD spectrum appears in the visible part of the spectrum (Fig. 2) in line with earlier observations^{2,4,45,48}. The generally accepted view is that the polythiophene undergoes a transition from an isolated disordered structure to a (semi-)microcrystalline aggregated structure in which the planarized polythiophene backbone stacks in a helical fashion giving rise to the strong CD response^{3,44,48–50}.

Harmonic light scattering. Second-harmonic scattering (SHS) and third-harmonic scattering (THS) are subsequently employed to study the internal structure during the aggregation process. SHS and THS are both nonlinear scattering techniques that require illumination of the sample in solution with a high-power laser. In contrast to linear scattering where photons scattered at the same frequency are detected, SHS and THS are processes for which scattering occurs at the double and triple frequency, respectively^{37,51–55}. The scattered intensity for SHS ($I_{2\omega}$) and THS ($I_{3\omega}$) depends on the square and cube of the incident intensity (I_ω), respectively. Both techniques are extremely sensitive to symmetry and aggregation state of the scatterers, and as such are very interesting tools to study aggregation or crystallization processes. The molecular nonlinear optical response is typically quantified by the first hyperpolarizability β for SHS and the second hyperpolarizability γ for THS. For molecular scatterers, the SHS and THS intensities are given by:^{51,52}

$$I_{2\omega} \sim N \langle \beta^2 \rangle I_\omega^2 \quad (1)$$

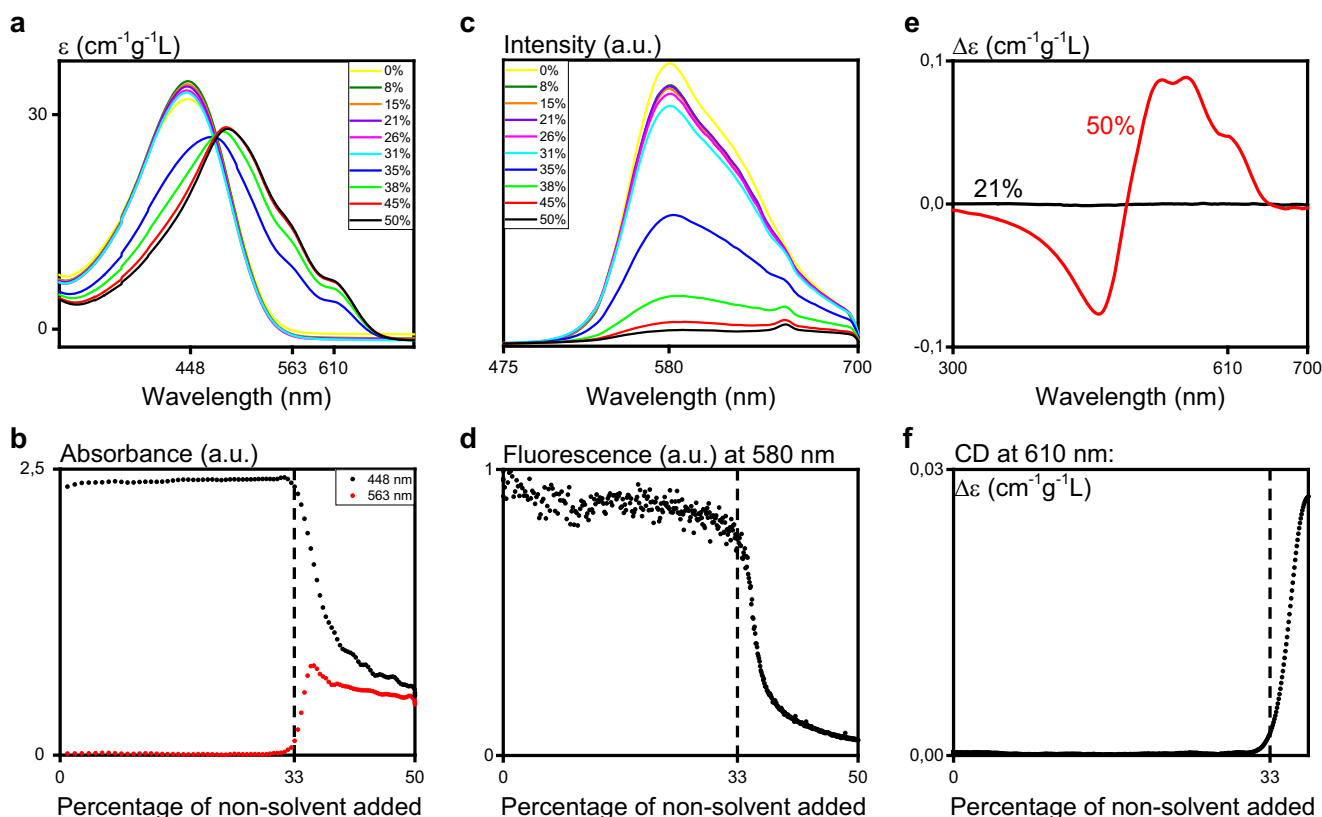


Fig. 2 Electronic spectroscopy of P3AT in chloroform. The addition of non-solvent methanol (0–50% v/v) is discrete for **a, c, e** and continuous for **b, d, f, a** Absorption spectra, shift of $\pi-\pi^*$ transition from 448 nm to 610 nm (upon aggregation a vibrational fine structure appears with the 0–0 transition at 610 nm and 0–1 transition at 563 nm) **b** absorbance at 448 nm (initial absorbance maximum) and 563 nm (vibrational fine structure of aggregate, initially not present), clear transition at 33% of non-solvent, compare with Fig. 2a **c** MPF spectra, peak maximum at 580 nm, excitation at 1300 nm. The smaller peak at 650 nm corresponds to SHS. **d** MPF intensity at 580 nm, decreases at 33% non-solvent, compare with Fig. 2c **e** CD at 21% (low methanol regime) and 50% of non-solvent added **f** CD intensity at 610 nm, first non-zero intensity at 33% non-solvent

$$I_{3\omega} \sim N \langle \gamma^2 \rangle I_{\omega}^3 \quad (2)$$

with N the concentration of scatterers and with the brackets denoting orientational averaging. For aggregated scatterers these equations can be written as^{51,52}:

$$I_{2\omega} \sim N' \langle (M \cdot f(\beta))^2 \rangle I_{\omega}^2 \quad (3)$$

$$I_{3\omega} \sim N' \langle (M \cdot f(\gamma))^2 \rangle I_{\omega}^3 \quad (4)$$

where in this case N' is the number of aggregates, M the number of molecules within each aggregate and $f(\beta)$ and $f(\gamma)$ represent specific combinations of molecular hyperpolarizability tensor components. It is noteworthy that for a mixture of non-aggregated and aggregated scatterers, the total SHS and THS intensities are additive. In fact, $(M \cdot f(\beta))$ and $(M \cdot f(\gamma))$ can be considered as effective hyperpolarizabilities of the aggregate. According to these relations and under the assumption that the molecules in the aggregate are oriented favorably with respect to each other, one can see that with an increase in the number of molecules within the aggregate, the harmonic scattering increases as well:

$$\begin{aligned} N' \sim \frac{N}{M} \Rightarrow N' \langle (M \cdot f(\beta))^2 \rangle &\sim \frac{N}{M} \langle (M \cdot f(\beta))^2 \rangle \sim M \cdot N \langle \beta^2 \rangle \\ &\Rightarrow M \uparrow \leftrightarrow I_{2\omega} \uparrow \end{aligned} \quad (5)$$

Both techniques are complementary in the sense that SHS can only be observed from noncentrosymmetric systems while there are no symmetry restrictions for THS. As a particular exception, $f(\beta) = 0$ for centrosymmetric aggregates. Note also that close to absorption (under resonant conditions) both hyperpolarizabilities can be significantly enhanced⁵¹. Additional information can be obtained from the depolarization ratio, which is the ratio of the intensity of vertically ($I_z(2\omega)$) to horizontally ($I_x(2\omega)$) polarized scattered light, which yields accurate information on the symmetry point group of the scatterers^{51,52}:

$$\rho_{SHS} = \frac{\langle I_z(2\omega) \rangle}{\langle I_x(2\omega) \rangle} \quad (6)$$

$$\rho_{THS} = \frac{\langle I_z(3\omega) \rangle}{\langle I_x(3\omega) \rangle} \quad (7)$$

For a dipolar scatterer with one dominating hyperpolarizability component, the depolarization ratio of SHS ρ_{SHS} is 5, whereas an octupolar scatterer has a ρ_{SHS} of 1.5⁵¹. For an isotropic scatterer the depolarization in THS ρ_{THS} is infinite, while for more ordered scatterers ρ_{THS} can be as low as 1.6⁵⁵.

The combination of both SHS and THS will give more information on the symmetry of the scatterers as changes in scattering intensity during growth for SHS and THS do not necessarily have to follow the same path. Further, the possible depolarizations for THS occur over a much wider range than those of SHS and in this respect THS can be more sensitive to symmetry changes. Nevertheless, both are measured with the same experimental setup and can be captured simultaneously.

Both SHS and THS are often accompanied by MPF, which is usually considered as an unwanted by-signal that can potentially obscure the SHS or THS signal. However, by carefully choosing the excitation wavelength it can also be considered as an extra tool to characterize the system under investigation.

Interestingly, the SHS response increases already dramatically upon addition of very small amounts of methanol (Fig. 3a), which continues to increase upon addition of non-solvent in the entire low methanol regime. Although the SHS signal is collected on

resonance (at 450 nm), the overall SHS response is still relatively weak because P3AT does not exhibit the typical Donor- π -Acceptor motif that is usually required for strong SHS responses. In any case, the SHS signal is always much higher than that of the solvent or solvent/mixture (Supplementary Fig. 1) and all properties (strength, depolarization) of the SHS signal relate to P3AT and not the solvent. Measurements conducted away from resonance (at 433 nm) follow a similar trend but the signal is much weaker. Nevertheless, this increase in SHS can only be explained by an increase in hyperpolarizability β of the monomer or by an aggregation process (or a combination of both). Indeed, for an ensemble of monomers the SHS intensity $I_{2\omega}$ is proportional to the concentration N and to the orientationally averaged of the square of the hyperpolarizability β . A change in the molecular hyperpolarizability β would require a conformational change of the polymer backbone. Changes in the conformation of the side chains would not be picked up since they only exhibit weak nonlinear optical activity. Since UV/Vis absorption and MPF clearly indicate that no conformational changes in the backbone occur in the low methanol regime, this option is overruled. One could argue that the dielectric constant of the system could have an influence on the hyperpolarizability of the P3AT, but these effects are small and could not account for the strong increase in SHS⁵⁶. Furthermore, solvent effects would show up in absorption and emission spectra as well. The only other possibility is that clustering occurs and that the total signal intensity results from a mixture of monomers and clusters in this early regime. With clusters we refer to precursor species composed of a loose ensemble of polymer chains and solvent molecules that exist before nucleation (and finally aggregation) and that are not yet in a planarized conjugated conformation. Furthermore, we must assume that no electronic coupling between polymer backbones is present in the clusters, since this would affect UV/Vis, emission and CD spectra. Also infrared (IR) and spectra in the low MeOH regime do not reveal any type of interaction (Supplementary Fig. 2). In this case, the total SHS intensity would be the sum of the monomer contribution and the cluster contribution.

The fact that clustering occurs in the low methanol regime is further corroborated by the following observations. For a solution containing 15% of methanol, we measured the SHS intensity vs. concentration of polymer. In the absence of changes in backbone conformation, which is the case, we should observe a linear dependence. However, we observed very strong deviations from linearity which can only be explained by clustering effects (Supplementary Fig. 3). Second, even in the low methanol regime, DLS measurements clearly indicate the formation of two species, one with a size of a few nanometer (corresponding to isolated polymer chains)⁵⁷ and one with sizes in the order of several hundreds of nanometers (Supplementary Fig. 4). Furthermore, the size of these clusters increases upon the addition of more non-solvent in the low methanol regime (Fig. 3c).

As SHS can only be observed if the scatterers are noncentrosymmetric, it must moreover be concluded that the clusters that are formed are not isotropic or amorphous. Although the asymmetric carbon in the alkyl side chains of the polythiophene do break the centrosymmetry, this is not sufficient to induce the SHS signal if the polymers are present in an isotropic cluster, and an additional breaking of symmetry is necessary⁵¹. Therefore, it is informative to have a look at the depolarization ratio. This simple metric measures the ratio between SHS light generated between parallel ($I_z(2\omega)$) and crossed ($I_x(2\omega)$) polarizers, and gives insight in the symmetry of the scattering species. In general, the hyperpolarizability can be decomposed in a polar and an octupolar part and the ratio of both parts determines the magnitude of the depolarization ratio. In absence of the polar

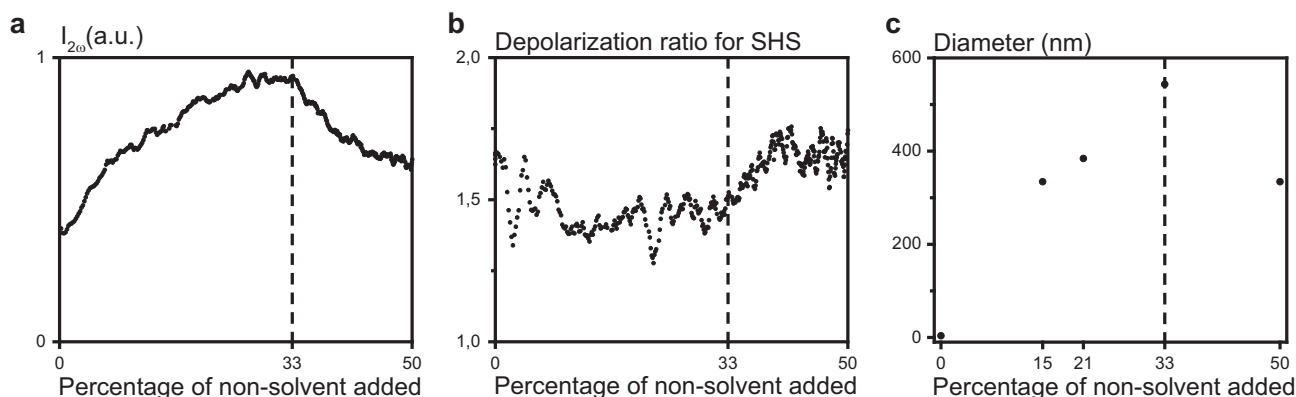


Fig. 3 Second-harmonic spectroscopy and dynamic light scattering of P3AT. **a** SHS intensity ($I_{2\omega}$ at 450 nm) vs. percentage of methanol added. The data are corrected for self-absorption and dilution. **b** Depolarization ratio of SHS vs. percentage of methanol added. **c** Average size of largest scatterers from DLS data

part, the depolarization reduces to 1.5, which is exactly the value that we observe. The molecular point groups that are compatible with a purely octopolar response are furthermore limited to the chemical topologies D_n , D_{2d} , D_{3h} , and T_d . Hence, a model that is compatible with these observations is the formation of structured clusters of loosely connected polymer chains. Furthermore, the polymer chains in the cluster are not planarized nor electronically coupled, but they are organized in an octopolar noncentrosymmetric structure. These clusters almost certainly contain solvent molecules preventing them to electronically couple. We hypothesize that these clusters are near isotropic and very dynamic entities in which symmetry is slightly broken at any point in time, with no well-defined structure. One could argue that depolarization ratios are not valid for larger scatterers. However, in the low methanol regime this is not an issue if the observed clusters are loosely bound polymer/solvent entities with a very dynamic structure and no clear phase boundary. In the high MeOH regime, one could expect deviations. However, the fact that the depolarization ratios of SHS and THS will be affected differently when surface and bulk effects come into play, which we do not observe, we assume that the depolarization ratios are still valid³⁶. Further, if the SHS response originates solely from the bulk, the depolarization ratio will still reflect the point group symmetry in the same way it would for a single molecule.

Interestingly, Van Cleuvenbergen et al.⁵⁸ observed similar effects in a poly(phenanthrene) that was studied by SHS. Although that study was less elaborate than this one, the authors already raised the possibility of orientationally correlated polymer chains before the actual aggregation but concluded this to be unlikely⁵⁸. SHS studies on a similar poly(alkyl)thiophene in pure chloroform yielded depolarization ratios of 1.5, which was attributed to the polythiophene in a random-coil-like configuration⁵⁹. To the best of our knowledge, aggregation effects in these systems have not yet been studied by nonlinear light scattering.

We also attempted THS measurements (excitation at 1300 nm, detection at 433 nm) in the low methanol regime. THS has a cubic dependence on the incident intensity and is usually much weaker than SHS. At the used polymer concentration and signal response time, no signal was detected in the low methanol regime. This can be attributed to the fact that the polymer backbone is not yet in an extended conjugated configuration and therefore the second hyperpolarizability γ is too low to yield a detectable signal at the relatively low polymer concentration used. However, at higher polymer concentrations (0.26 mg mL^{-1}) and longer signal acquisition time we were able to detect a THS signal (Fig. 4a inset). An increase in THS signal upon addition of non-solvent solution can clearly be observed, even at relatively low methanol

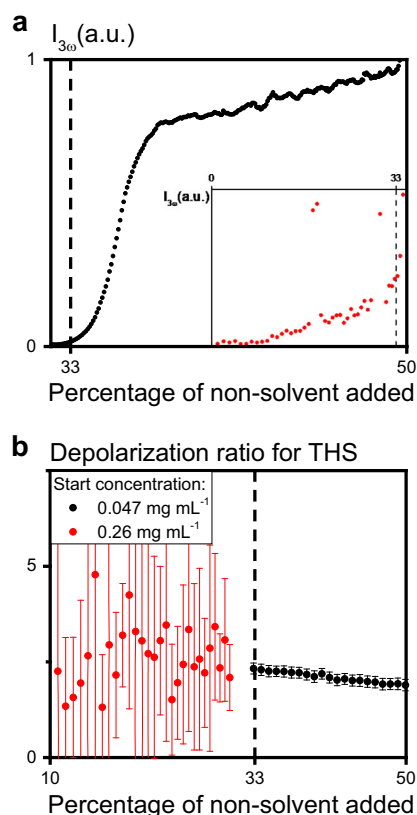


Fig. 4 Third-harmonic scattering of P3AT. **a** THS intensity ($I_{3\omega}$ at 433 nm) vs. amount of methanol added for a polymer concentration of 0.047 mg mL^{-1} . The inset is the THS intensity at the low methanol regime for a polymer concentration of 0.26 mg mL^{-1} and longer acquisition time. All data were corrected for self-absorption and dilution. **b** Depolarization ratio for THS vs. percentage of methanol added. The red dots represent the depolarization ratio observed for a polymer concentration of 0.26 mg mL^{-1} , the black dots for a polymer concentration of 0.047 mg mL^{-1} . The average depolarization ratio is within the error for the overall process (error calculated from the CI of the THS intensities for vertical and horizontal polarization). For the low methanol regime, the error is large as the signal intensity is low

concentration. Moreover, upon overlaying SHS and THS, one can see that the growth kinetics observed with SHS and THS are identical (Supplementary Fig. 5), which indicates that the observed responses originates from one type of clusters. However

this does not preclude the presence of other types of clusters that do not exhibit an appreciable SHS/THS response. The depolarization ratio for THS was on average 2, consistent with a structure that is not isotropic (in that case the depolarization would be infinite) (Fig. 4b). In fact, such a low depolarization ratio is indicative of scatterers that can support a hexadecapolar charge distribution⁵⁵.

Upon further addition of methanol (>33%) up to the point where the absorption starts to red-shift, the SHS intensity slightly decreases. This decrease is attributed to a change in resonance enhancement (shift in absorbance) but also the conformational change of the polymer backbone will affect the overall SHS signal (Fig. 3a). THS on the other hand strongly increases (Fig. 4a). This is consistent with the accepted view that aggregates are formed in which the backbone of the polymer is planarized with increased conjugation^{21,60}. Such strongly conjugated systems are known to exhibit very high second hyperpolarizabilities⁶¹. However, the most interesting part is that the depolarization for both SHS and THS does not change much upon aggregation and planarization. For SHS there is a small increase indicating the presence of some polarity, which might be due to dangling polymer parts of the polymer chain (Fig. 3b), whereas the depolarization of THS does not change significantly (Fig. 4b). This indicates that the transformation from clusters in the low methanol regime to the final aggregate is not accompanied by a dramatic change in symmetry. Hence, a plausible view of the entire process is that at low methanol concentration dense polymer-solvent clusters are formed in which extended but not fully conjugated polymer chains already adopt a similar structure in terms of symmetry as the final aggregates. Remarkably, these clusters already form upon addition of very small amounts of methanol (<10%). The size of these clusters is slightly larger than the final aggregate since solvent molecules are present, that prevent the polymers from electronic coupling, and since the conformational flexibility in the non-planarized state is higher. However, upon addition of more methanol, solvent is expelled from the structure, the backbone is allowed to planarize, and the final aggregates are formed. It is well-known that (chiral) polythiophene tends to adopt a (helical) supramolecular structure of stacked planarized polymer chains and the observed depolarization ratios are consistent with such a structure⁶². However, the depolarization does not allow us to infer the shape of the aggregates. The combination of isotropic, octopolar and hexadecapolar contributions to the nonlinearity tensors of SHS and THS can only exclude certain types of symmetries. A helical structure is one of several symmetries that

is compatible with these conditions as described by Ford and Andrews⁵⁴. Interestingly, particle size as measured by DLS indicates the formation of slightly smaller aggregates upon planarization, consistent with the more dense packing in the planar conformation and solvent that is expelled from the clustering entities (Fig. 3c). The clusters in the low methanol regime act as separate pre-organized micro-environments. Not only the interaction between solute and solvent affects the aggregation process but also the miscibility of solvent and non-solvent has a great influence. Hence, a careful choice of solvent and non-solvent could allow fine tuning of the structure of the final aggregate. In fact, there are a number of reports in literature that confirm this hypothesis^{1,43,44,63}. Further, IR and Raman spectra confirm that there are no indications for interactions between the polymer chains (Supplementary Fig. 2). A schematic representation of this process is displayed in Fig. 5.

To confirm our hypothesis, we performed an aggregation experiment by lowering solvent quality with temperature instead of the introduction of a (second) (non-)solvent to the polymer system. Hexanol is a non-solvent for P3AT at room temperature, but at elevated temperatures (120 °C), small amounts of polymer can be dissolved. Upon cooling down, P3AT will start to aggregate at 75 °C. Before supramolecular aggregation sets in, we did not observe any change in SHS and THS, suggesting that in this case no clusters are formed. This corroborates our hypothesis since there is no good solvent available to induce polymer-solvent clusters. At lower temperature, supramolecular aggregation sets in and both SHS and THS start to increase suddenly (see Fig. 6a), consistent with the formation of aggregates. However, the final aggregates are different as compared to those obtained by the addition of non-solvent. The depolarization ratio was found to be 2.3 for SHS and 5 for THS (Fig. 6b), significantly different from those obtained by adding non-solvent (1.5 and 2, respectively). Although these numbers do not allow us to extract exact structural information they indicate that the structure of the formed aggregates is significantly different from those obtained in the solvent/non-solvent system. Comparing the CD spectra of the final aggregates for both systems does indeed show differences between both types of aggregates (Fig. 6c). Nevertheless, the depolarization ratios together with CD still suggest a very similar structure. Possibly the higher depolarization ratios and stronger CD are due to a more defective structure which one could expect for a supramolecular aggregation that is not preceded by clusters.

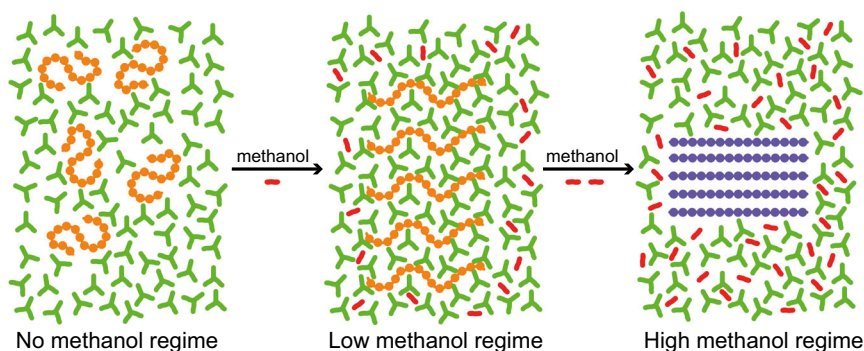


Fig. 5 Schematic representation of the supramolecular aggregation process of P3ATs from single chain to helical aggregate. Initially, P3AT chains are dissolved in chloroform (good solvent). Upon addition of methanol (non-solvent for P3AT) chains assemble into structured micro-environments/clusters. Chloroform molecules between the single chains prevent the chains from planarizing. For a certain amount of methanol added, chloroform is expelled from the cluster causing the polymer backbone to planarize. The ordered structure present in the clusters is preserved during aggregation. The conformational change of the polymer backbone results in a red-shift and a bisignate CD response for these particular P3ATs. (In this representation, only the formation of clusters and aggregates is presented. Smaller species in equilibrium are omitted for clarity.)

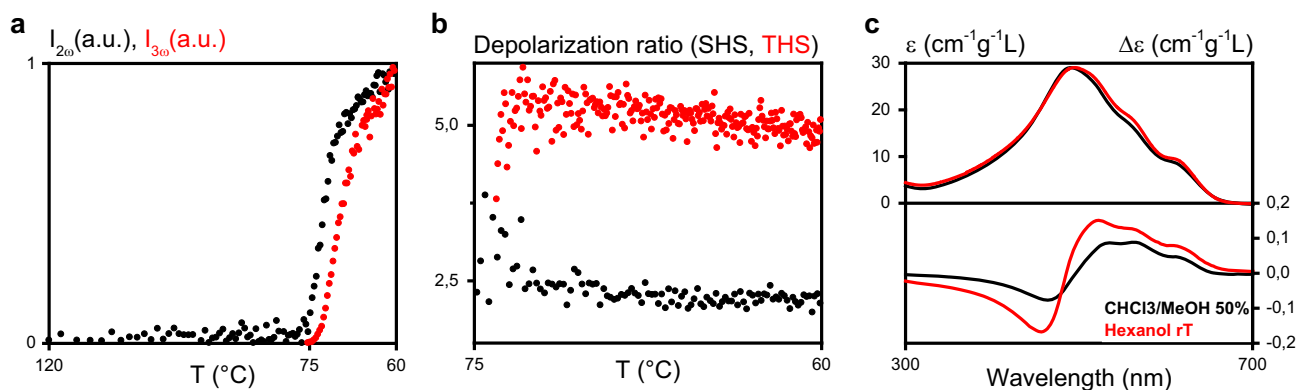


Fig. 6 Lowering solvent quality by decreasing temperature (P3AT in hexanol). **a** SHS (I_{20} , at 400 nm, black) and THS (I_{30} , at 433 nm, red) intensities are both increasing following a similar trend as aggregation sets in at 75 °C. **b** Corresponding depolarization ratios starting at 75 °C. **c** Absorbance (upper) and CD (bottom) spectra for aged aggregates: 50% solvent/non-solvent system (black) and non-solvent/T regime (red) at room temperature (rT, 20 °C)

Our observations for the solvent/non-solvent system are in line with a growing body of research demonstrating the occurrence of supramolecular species in conditions preceding crystallization. Indeed, the formation of large mesoscopic clusters precedes the organization into ordered (semi-)microcrystalline aggregates through desolvation and planarization of the polymer backbone. As mentioned in the introduction, currently two main models describe the involvement of supramolecular precursor species in nonclassical crystallization pathways. Within the two-step nucleation model, the initial clusters form a separate phase of liquid-like clusters with increased concentration of monomeric species, after which nucleation and growth occur classically within this new phase. Two-step nucleation offers a compelling explanation for several experimental observations in proteins³⁰ and is often assumed valid for small organic molecules as well^{64,65}, but its general applicability has been questioned lately^{26,32}. Alternatively, in the pre-nucleation cluster pathway clusters are in equilibrium with the surrounding solution and formally do not represent a separate phase^{24,25,66}. Also, pre-nucleation clusters may have internal structure resembling that of the nascent crystal phase, in contrast with the liquid droplets formed in the two-step model which are (at least initially) expected to be isotropic in nature. The fact that combined SHS and THS experiments imply that the internal structure in the P3AT clusters is similar to the structure observed in the (semi-)microcrystalline aggregates in the high methanol regime, is a strong indication that our observations fit within the framework of the pre-nucleation pathway. To further distinguish between these possibilities, we have performed time-resolved SHS measurements where we added a certain amount of methanol (15%) to induce clustering well within the low methanol regime, and measured the SHS response over a period of one hour. In case the observed clusters would form a separate phase as in the two-step model, they would be expected to undergo coalescence (oiling out). No change in SHS signal was observed, suggesting that the clusters are indeed in equilibrium with their surroundings and do not form a separate phase. Finally, we found that filtering the solution with a 0.2 μm Teflon filter had no effect on the SHS signal. This is in line with experiments carried out by Jawor-Baczynska et al.⁶⁷, who studied the appearance of large (100–300 nm) clusters of amino-acids in aqueous solution. They concluded that this implies that the clusters cannot be solid nanoparticles but must be liquid-like solution species.

In conclusion, we have investigated the supramolecular aggregation of the regioregular P3AT triggered by lowering the solvent quality by two independent methods: adding a non-solvent and lowering the temperature. To fully reveal the complete aggregation mechanism, we used a combination of harmonic light scattering

techniques that are able to monitor aggregation effects that remain invisible to most classical characterization techniques. Our main conclusion is that, even well before the actual formation of (semi-)microcrystalline aggregates as evidenced by electron spectroscopy (absorption and emission), the polymer is already present as ordered polymer-solvent clusters in a solvent/non-solvent system. Furthermore, the symmetry of these clusters is very similar to that of the final (semi-)microcrystalline aggregates. This and the fact that the clusters appear to be in equilibrium with the surrounding solution is in line with the pre-nucleation cluster model.

Methods

P3AT. In our experiments we used a regioregular poly(3-(3(S),7-dimethyloctyl) thiophene) of 34 monomeric units (8.2 kDa) and dispersity 1.1 (Fig. 1) that was reported by Van den Eede et al.² using a Ni(bis(diphenylphosphino)propane)-mediated Kumada catalyst transfer condensative polymerization reaction. We opted for this particular polymer as it can serve as a model system for many other polythiophene derivatives that have been investigated for applications. The fact that it is chiral allows us to use CD as an extra characterization tool.

Supramolecular aggregation. The polymer was dissolved in chloroform, which is a good solvent, and methanol was used as a non-solvent to lower the solvent quality (Supplementary Table 1) and induce aggregation. The initial concentration of the polymer was 0.047 mg mL⁻¹, unless stated otherwise. The supramolecular aggregation process was continuously monitored separately by UV/Vis, CD, SHS, THS and MPF under addition of non-solvent. Methanol was added dropwise to the chloroform with a syringe pump (1.18 $\mu\text{L s}^{-1}$ or 50% (v/v) non-solvent in 15.6 min) in a 1 cm cuvette while stirring, which was necessary to obtain a homogenous solution.

For the experiments in 1-hexanol, which is a non-solvent for P3AT at room temperature, 0.047 mg mL⁻¹ of polymer was dissolved by heating to 120 °C using a temperature-controlled cell holder. The supramolecular aggregation was monitored continuously by UV/Vis, CD, SHS, THS, and MPF upon (passively) cooling down to room temperature.

Electronic spectroscopy. UV/Vis absorption data were recorded on a Perkin Elmer lambda 900 spectrometer or a Jasco V-730 spectrometer. All CD spectra were measured on a Jasco J-810 spectrometer. DLS measurements were executed on a Brookhaven BI-90Plus Particle Size Analyzer with a laser wavelength of 659 nm, collecting of the scattered light at an angle of 90° and an acquisition time of 120 s.

Vibrational spectroscopy. IR spectra were recorded on a Bruker Vertex 70 spectrometer with 4000–400 cm⁻¹ range and resolution of 1 cm⁻¹. Raman spectra were recorded on a Bruker Vertex 70 with Raman module Bruker RAM II with spectral range within 5000–50 cm⁻¹. The RAM II module is equipped with a standard 1064 nm laser (300 mW used) and resolution of 2 cm⁻¹.

Harmonic light scattering. For THS, SHS, and MPF, we used a home-made harmonic scattering setup⁵² (Fig. 7). As a high-power light source, we used a tunable Spectra-Physics Insight DeepSee femtosecond pulsed laser. A Glan-Taylor polarizer ensures linearly polarized light oscillating in the z-direction, perpendicular to the optical table. The light is subsequently focused into the polymer solution which was placed in a standard quartz cuvette (1 cm optical path length).

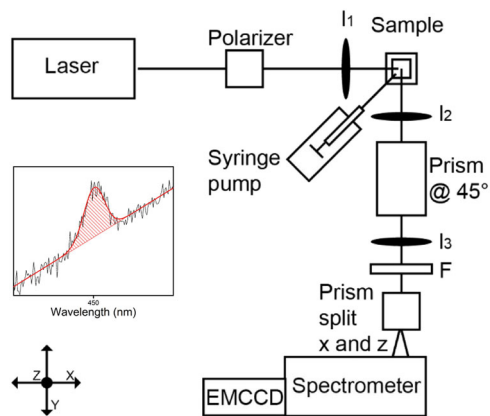


Fig. 7 Schematic representation of second- and third-harmonic scattering setup. A femtosecond pulse laser is used to illuminate the sample. Scattering is collected at a 90° angle. The sample holder includes a stirring device and a syringe pump is installed for slow addition of non-solvent. And a typical HLS signal can include MPF. This is eliminated by curve fitting with the combination of a Gaussian and linear curve function. The shaded area is the total signal response

The beam waist is $\sim 8 \mu\text{m}$ resulting in a Rayleigh length of $\sim 190 \mu\text{m}$ ⁵². Particles smaller than $1 \mu\text{m}$ fit well within the focal point. The harmonic light (and MPF) is collected, collimated and then focused onto the slit of a Bruker Surespectrum 500 is spectrometer attached to an EMCCD Ixon 897 Andor camera. A 150/300 grating in the spectrometer enables us to record second and third-harmonic light scattering and MPF. A Wollaston prism is mounted in front of the spectrometer to split the scattered light in its vertically (I_z) and horizontally (I_x) polarized components. This allows us to simultaneously record the depolarization ratio. Before each measurement, the polarization response of the optical system is verified with disperse red 1 and the obtained depolarization values are fully consistent with those reported in literature, typically 3.5 (see e.g. Hubbard et al.⁶⁸).

The advantage of the spectral setup and the use of the charge-coupled device camera is that any contribution from MPF to the SHS or THS signal can be eliminated by curve fitting. The direct region around the signal peak area can be fitted using the combination of a Gaussian and a linear fitting function as the MPF can be considered linear for this small data interval (red line Fig. 7). The area under the peak (red shaded area) is the total, in this case SHS, response.

In principle, THS, SHS, and MPF can be measured simultaneously. However, due to the strong absorbance and emission of the polythiophene in the visible part of the spectrum, we have tried to avoid excessive self-absorption of the SHS and THS signals and interference with MPF. Therefore, we opted for an excitation wavelength of 900 nm to record SHS data and 1300 nm to record THS data. Off-resonance SHS was executed at 866 nm. Data acquisition times were always 2 s, unless noted otherwise.

All the reported data are corrected for the influence of dilution and the change in self-absorbance of the scatterers upon addition of non-solvent. (Non-)solvents have very weak hyperpolarizabilities compared to P3AT and therefore the signal of P3AT is dominating in all regions during measurements (Supplementary Fig. 1).

Data availability

The data that support the findings of this study are available from the corresponding author M.M. upon reasonable request.

Received: 2 July 2019; Accepted: 17 October 2019;

Published online: 13 November 2019

References

- Goto, H., Okamoto, Y. & Yashima, E. Solvent-induced chiroptical changes in supramolecular assemblies of an optically active, regioregular polythiophene. *Macromolecules* **35**, 4590–4601 (2002).
- Van Den Eede, M. P. et al. The influence of the end-group on the chiral self-assembly of all-conjugated block copolymers. *Polym. Chem.* **8**, 5666–5672 (2017).
- Kiriya, N. et al. One-dimensional aggregation of regioregular polyalkylthiophenes. *Nano Lett.* **3**, 707–712 (2003).
- Goto, H., Yashima, E. & Okamoto, Y. Unusual solvent effects on chiroptical properties of an optically active regioregular polythiophene in solution. *Chirality* **12**, 396–399 (2000).
- Kajiya, D., Ozawa, S., Koganezawa, T. & Saitow, K. I. Enhancement of out-of-plane mobility in P3HT film by rubbing: Aggregation and planarity enhanced with low regioregularity. *J. Phys. Chem. C* **119**, 7987–7995 (2015).
- Vandendriessche, S., Willot, P., Valev, V. K., Koeckelberghs, G. & Verbiest, T. Optical second harmonic generation in a low-bandgap polymer. *Mater. Chem. Phys.* **147**, 356–359 (2014).
- Surin, M. et al. Oligothiophene-based nanostructures: from solution to solid-state aggregates. *Synth. Met.* **147**, 67–72 (2004).
- Matthews, J. R., Goldoni, F., Schenning, A. P. H. J. & Meijer, E. W. Non-ionic polythiophenes: a non-aggregating folded structure in water. *Chem. Commun.* 5503–5505 (2005).
- Leclère, P. et al. About oligothiophene self-assembly: from aggregation in solution to solid-state nanostructures. *Chem. Mater.* **16**, 4452–4466 (2004).
- Koppe, M. et al. Influence of molecular weight distribution on the gelation of P3HT and its impact on the photovoltaic performance. *Macromolecules* **42**, 4661–4666 (2009).
- Yamamoto, T. et al. Extensive studies on π -stacking of poly(3-alkylthiophene-2,5-diyl) and poly(4-alkylthiazole-2,5-diyl)s by optical spectroscopy, NMR analysis, light scattering analysis, and X-ray crystallography. *J. Am. Chem. Soc.* **120**, 2047–2058 (1998).
- Verswyvel, M., Goossens, K. & Koeckelberghs, G. Amphiphilic chiral block-poly(thiophene)s: tuning the blocks. *Polym. Chem.* **4**, 5310–5320 (2013).
- Deckers, S. et al. Poly(3-alkylthiophene)s show unexpected second-order nonlinear optical response. *Chem. Commun.* **50**, 2741–2743 (2014).
- Jaymand, M., Hatamzadeh, M. & Omid, Y. Modification of polythiophene by the incorporation of processable polymeric chains: recent progress in synthesis and applications. *Prog. Polym. Sci.* **47**, 26–69 (2015).
- Park, Y. D. et al. Solubility-induced ordered polythiophene precursors for high-performance organic thin-film transistors. *Adv. Funct. Mater.* **19**, 1200–1206 (2009).
- Chang, M., Lim, G. T., Park, B. & Reichmanis, E. Control of molecular ordering, alignment, and charge transport in solution-processed conjugated polymer thin films. *Polym. (Basel)* **9**, 23–31 (2017).
- Wang, H. et al. Structure and morphology control in thin films of conjugated polymers for an improved charge transport. *Polym. (Basel)* **5**, 1272–1324 (2013).
- Rughooputh, S. D. D. V., Bloor, D., Phillips, D. & Movaghar, B. One-dimensional exciton diffusion in a conjugated polymer. *Phys. Rev. B* **35**, 8103–8112 (1987).
- Agbolaghi, S. & Zenoozi, S. A comprehensive review on poly(3-alkylthiophene)-based crystalline structures, protocols and electronic applications. *Org. Electron. Phys. Mater. Appl.* **51**, 362–403 (2017).
- Bouman, M. M. & Meijer, E. W. Stereomutation in optically active regioregular polythiophenes. *Adv. Mater.* **7**, 385–387 (1995).
- Reynolds, J. R., Thompson, B. C. & Skotheim, T. A. *Handbook of Conducting Polymers, Fourth Edition* (CRC Press, 2019).
- Vekilov, P. G. Nucleation of protein crystals. *Prog. Cryst. Growth Charact. Mater.* **62**, 136–154 (2016).
- De Yoreo, J. J. Principles of crystal nucleation and growth. *Rev. Mineral. Geochem.* **54**, 57–93 (2005).
- Gebauer, D., Kellermeier, M., Gale, J. D., Bergström, L. & Cölfen, H. Pre-nucleation clusters as solute precursors in crystallisation. *Chem. Soc. Rev.* **43**, 2348–2371 (2014).
- Gebauer, D. & Wolf, S. E. Designing solid materials from their solute state: a shift in paradigms toward a holistic approach in functional materials chemistry. *J. Am. Chem. Soc.* **141**, 4490–4504 (2019).
- Sleutel, M. & Van Driessche, A. E. S. Nucleation of protein crystals—a nanoscopic perspective. *Nanoscale* **10**, 12256–12267 (2018).
- Vekilov, P. G. The two-step mechanism of nucleation of crystals in solution. *Nanoscale* **2**, 2346–2357 (2010).
- Xiao, Z. et al. Phase transformation of GeO₂ gas nanocrystals under ambient conditions. *Nano Lett.* **18**, 3290–3296 (2018).
- Maes, D. et al. Do protein crystals nucleate within dense liquid clusters? *Acta Crystallogr. Sect. Struct. Biol. Commun.* **71**, 815–822 (2015).
- Vekilov, P. G. Nucleation of protein crystals. *Prog. Cryst. Growth Charact. Mater.* **62**, 136–154 (2016).
- Li, D., Nielsen, M. H. & De Yoreo, J. J. Design, fabrication, and applications of in situ fluid cell TEM. *Methods Enzymol.* **532**, 147–164 (2013).
- Van Driessche, A. E. S. et al. Molecular nucleation mechanisms and control strategies for crystal polymorph selection. *Nature* **556**, 89–94 (2018).
- Schiener, A. et al. In situ investigation of two-step nucleation and growth of CdS nanoparticles from solution. *Nanoscale* **7**, 11328–11333 (2015).
- Hendrickx, E., Clays, K. & Persoons, A. Hyper-Rayleigh scattering in isotropic solution. *Acc. Chem. Res.* **31**, 675–683 (1998).
- Revillod, G. et al. Multipolar contributions to the second harmonic response from mixed DiA-SDS molecular aggregates. *J. Phys. Chem. C* **112**, 2716–2723 (2008).

36. Van Cleuvenbergen, S. et al. Morphology and structure of ZIF-8 during crystallisation measured by dynamic angle-resolved second harmonic scattering. *Nat. Commun.* **9**, 3418 (2018).
37. Roke, S. & Gonella, G. Nonlinear light scattering and spectroscopy of particles and droplets in liquids. *Annu. Rev. Phys. Chem.* **63**, 353–378 (2012).
38. Aguiar, H. B. De, Beer, A. G. F. De & Roke, S. The presence of ultralow densities of nanocrystallites in amorphous poly(lactic acid) microspheres. *J. Phys. Chem. B* **8**, 8906–8910 (2013).
39. Correa-Soto, C. et al. Second harmonic generation microscopy as a tool for the early detection of crystallization in spray dried dispersions. *J. Pharm. Biomed. Anal.* **146**, 86–95 (2017).
40. Dewalt, E. L. et al. Polarization-resolved second-harmonic generation microscopy as a method to visualize protein-crystal domains. *Acta Crystallogr. Sect. D. Biol. Crystallogr.* **69**, 74–81 (2013).
41. Hendrickx, E. et al. Quadratic nonlinear optical properties of correlated chromophores: cyclic 6,6'-dinitro-1,1'-binaphthyl-2,2'-ethers. *Chem. Phys. Lett.* **270**, 241–244 (1997).
42. Kelley, A. M. A multimode vibronic treatment of absorption, resonance Raman and hyper-Rayleigh scattering of excitonically coupled molecular dimers. *J. Chem. Phys.* **119**, 3320–3331 (2003).
43. Langeveld-Voss, B. M. W., Christiaans, M. P. T., Janssen, R. A. J. & Meijer, E. W. Inversion of optical activity of chiral polythiophene aggregates by a change of solvent. *Macromolecules* **31**, 6702–6704 (1998).
44. Potai, R., Kamphan, A. & Traiphol, R. Conformational change, intrachain aggregation and photophysical properties of regioregular poly(3-octylthiophene) in alkanes. *J. Polym. Sci. Part B Polym. Phys.* **51**, 1288–1297 (2013).
45. Hattori, S., Vandendriessche, S., Koeckelberghs, G., Verbiest, T. & Ishii, K. Evaporation rate-based selection of supramolecular chirality. *Chem. Commun.* **53**, 3066–3069 (2017).
46. Scharisch, C. et al. Control of aggregate formation in poly(3-hexylthiophene) by solvent, molecular weight, and synthetic method. *J. Polym. Sci. Part B Polym. Phys.* **50**, 442–453 (2012).
47. Johnson, C. E. & Boucher, D. S. Poly(3-hexylthiophene) aggregate formation in binary solvent mixtures: an excitonic coupling analysis. *J. Polym. Sci. Part B Polym. Phys.* **52**, 526–538 (2014).
48. Van Den Bergh, K., Cosemans, I., Verbiest, T. & Koeckelberghs, G. Expression of supramolecular chirality in block copoly(thiophene)s. *Macromolecules* **43**, 3794–3800 (2010).
49. Potai, R., Kamphan, A. & Traiphol, R. On the formation of non-emissive and emissive aggregates of regioregular poly(3-octylthiophene) in different local environments. *Synth. Met.* **187**, 136–144 (2014).
50. Shibaev, P. V. & Schaumburg, K. Conformational transitions in chiral polythiophenes. *Synth. Met.* **124**, 291–294 (2001).
51. Verbiest, T., Clays, K. & Rodriguez, V. *Second-order Nonlinear Optical Characterization Techniques* (CRC Press, 2009).
52. Van Steerteghem, N., Clays, K., Verbiest, T. & Van Cleuvenbergen, S. Third-harmonic scattering for fast and sensitive screening of the second hyperpolarizability in solution. *Anal. Chem.* **89**, 2964–2971 (2017).
53. Clays, K., Hendrickx, E., Triest, M. & Persoons, A. Second-order nonlinear optics in isotropic liquids: Hyper-Rayleigh scattering in solution. *J. Mol. Liq.* **67**, 133–155 (1995).
54. Ford, J. S. & Andrews, D. L. Molecular tensor analysis of third-harmonic scattering in liquids. *J. Phys. Chem. A* **122**, 563–573 (2018).
55. Rodriguez, V. Polarization-resolved third-harmonic scattering in liquids. *J. Phys. Chem. C* **121**, 8510–8514 (2017).
56. Woodford, J. N., Pauley, M. A. & Wang, C. H. Solvent dependence of the first molecular hyperpolarizability of p-nitroaniline revisited. *J. Phys. Chem. A* **101**, 1989–1992 (1997).
57. Heffner, G. W., Pearson, D. S. & Gettinger, C. L. Characterization of poly(3-octylthiophene). I: molecular characterization in dilute solution. *Polym. Eng. Sci.* **35**, 860–867 (1995).
58. Van Cleuvenbergen, S. et al. Record-high hyperpolarizabilities in conjugated polymers. *J. Mater. Chem. C* **2**, 4533–4538 (2014).
59. Deckers, S. et al. Regioregularity increases second-order nonlinear optical response of polythiophenes in solution. *J. Phys. Chem. C* **119**, 18513–18517 (2015).
60. Qu, Y. et al. H-aggregated form II spherulite of poly(3-butylthiophene) grown from solution. *ACS Macro Lett.* **1**, 1274–1278 (2012).
61. Hales, J. M. et al. Design of organic chromophores for all-optical signal processing applications. *Chem. Mater.* **26**, 549–560 (2014).
62. Langeveld-Voss, B. M. W. et al. Investigation of exciton coupling in oligothiophenes by circular dichroism spectroscopy. *Adv. Mater.* **10**, 1343–1348 (1998).
63. Annunziata, O., Payne, A. & Wang, Y. Solubility of lysozyme in the presence of aqueous chloride salts: common-ion effect and its role on solubility and crystal thermodynamics. *J. Am. Chem. Soc.* **130**, 13347–13352 (2008).
64. Erdemir, D., Lee, A. Y. & Myerson, A. S. Nucleation of crystals from solution: Classical and two-step models. *Acc. Chem. Res.* **42**, 621–629 (2009).
65. Tsarfati, Y. et al. Crystallization of organic molecules: nonclassical mechanism revealed by direct imaging. *ACS Cent. Sci.* **4**, 1031–1036 (2018).
66. Mikhlin, Y., Karacharov, A., Likhatski, M., Podlipskaya, T. & Zizak, I. Direct observation of liquid pre-crystallization intermediates during the reduction of aqueous tetrachloroaurate by sulfide ions. *Phys. Chem. Chem. Phys.* **16**, 4538–4543 (2014).
67. Jawor-Baczynska, A., Moore, B. D., Lee, H. S., McCormick, A. V. & Sefcik, J. Population and size distribution of solute-rich mesospecies within mesostructured aqueous amino acid solutions. *Faraday Discuss.* **167**, 425–440 (2013).
68. Hubbard, S. F., Petschek, R. G. & Singer, K. D. Spectral content and dispersion of hyper-Rayleigh scattering. *Opt. Lett.* **21**, 1774–1776 (1996).

Acknowledgements

The authors acknowledge financial support from the fund for scientific research – Flanders (research grant G099319N) (T.V. and S.V.C.), (research grant G094717N – O.D. and C.B.), the Hercules Foundation (T.V., G.K., K.C.), the KU Leuven (C1 grant) (M.M., K.C., G.K., C.B., O.D.). S.V.C. also thanks FWO Flanders for his postdoctoral fellowship. The authors acknowledge the Solvomet Group (KUL) for IR and Raman measurements.

Author contributions

M.M. wrote the manuscript and conducted and analyzed the HLS and ES experiments, S.V.C., T.V. and K.C. designed the experiments, interpreted the experimental data, and proofread the manuscript. M.P.V.D.E. and G.K. performed the synthesis of the polymers and proofread the manuscript. O.D. and C.B. performed, analyzed, and interpreted the DLS data and proofread the manuscript.

Competing interests

The authors declare no competing interests.

Additional information

Supplementary information is available for this paper at <https://doi.org/10.1038/s42004-019-0230-4>.

Correspondence and requests for materials should be addressed to M.M. or S.V.C.

Reprints and permission information is available at <http://www.nature.com/reprints>

Publisher's note Springer Nature remains neutral with regard to jurisdictional claims in published maps and institutional affiliations.



Open Access This article is licensed under a Creative Commons Attribution 4.0 International License, which permits use, sharing, adaptation, distribution and reproduction in any medium or format, as long as you give appropriate credit to the original author(s) and the source, provide a link to the Creative Commons license, and indicate if changes were made. The images or other third party material in this article are included in the article's Creative Commons license, unless indicated otherwise in a credit line to the material. If material is not included in the article's Creative Commons license and your intended use is not permitted by statutory regulation or exceeds the permitted use, you will need to obtain permission directly from the copyright holder. To view a copy of this license, visit <http://creativecommons.org/licenses/by/4.0/>.

© The Author(s) 2019